



## Journal of Mining and Earth Sciences

Website: <http://jmes.humg.edu.vn>



# Numerical analysis of the tunnel uplift behavior subjected to seismic loading



Tan Manh Do <sup>1,2,\*</sup>, Anh Ngoc Do <sup>1</sup>, Hung Trong Vo <sup>1</sup>

<sup>1</sup> Faculty of Civil Engineering, Hanoi University of Mining and Geology, Vietnam

<sup>2</sup> Lulea University of Technology, Lulea, Sweden

### ARTICLE INFO

#### Article history:

Received 18<sup>th</sup> Aug. 2021

Revised 28<sup>th</sup> Nov. 2021

Accepted 18<sup>th</sup> Jan. 2022

#### Keywords:

Excess pore pressure,  
Liquefiable soils,  
Numerical analysis,  
Seismic loading,  
Tunnel uplift.

### ABSTRACT

*Seismic loading has always been a major concern for any engineering structures, and thereby, underground facilities (e.g., tunnels) are not exceptional. It is due to the seismically induced uplift and instability of tunnels caused by the large deformation of liquefiable soils. Therefore, the tunnel uplift behaviors subjected to seismic loading are always taken into account in any designing stages of tunnels. This study's main goal was to evaluate how a tunnel buried in liquefiable and non-liquefiable soils would behave when subjected to seismic stress. Seismic and liquefaction potential assessments of the soils surrounding the tunnel were carried out using the finite-element method. In this study, PM4sand, an advanced constitutive model was adopted in all finite-element models. In addition, the uplift displacement and excess pore pressure of liquefiable soils were studied, under a typical earthquake. Investigations were also conducted into how the thickness of the non-liquefiable soil affected seismic loading, tunnel uplift displacement, and the buildup of excess pore water pressure. As a result, during the earthquake, liquefaction was triggered in most parts of the sand layer but not in the clay layer. In addition, the tunnel uplift displacement was triggered due to the relative motion and interaction at both sides of the tunnel. In addition, this study found that the thickness of the non-liquefiable soil layer (sand layer) had a significant impact on the build-up of excess pore water pressure and, consequently, the tunnel uplift displacement. The uplift displacement and excess pore water pressure build-up were higher the thinner the non-liquefiable layer was.*

Copyright © 2022 Hanoi University of Mining and Geology. All rights reserved.

\*Corresponding author

E - mail: [domanhtan@khoaxaydung.edu.vn](mailto:domanhtan@khoaxaydung.edu.vn)

DOI: 10.46326/JMES.2022.63(3a).02

## 1. Introduction

One of the major concerns for tunnels buried in liquefiable soil is the uplift susceptibility under seismic loading. It is due to the fact that excess pore pressure in a saturated soil layer is generally built-up during earthquakes, which could lead to a decrease in effective stress and soil liquefaction. Large deformation of liquefiable soils may cause the uplift and instability of tunnels. Thereby, the tunnel uplift behaviors subjected to seismic loading are always taken into account in any designing stages of tunnels. During the past decade, behaviors of tunnels under dynamic conditions have been addressed in many studies by both numerical analyses (Azadi and Hosseini 2010; Hu et al. 2018; Lin et al. 2017; Liu and Song 2006; Sun et al. 2008; Unutmaz 2016; Zheng et al. 2021) and physical model tests (Adalier et al. 2003; Chou et al. 2011; Saeedzadeh and Hataf 2011; Tobita et al. 2011). Among these, Azadi and Hosseini (2010) performed a numerical study on tunnel uplift effects caused by soil liquefaction. In their study, a finite difference software, FLAC 2D, was used to evaluate the pore pressure changes during earthquakes with several considered parameters, e.g., tunnel diameters, buried depths, and soil strengths. In the study by Lin et al. (2017), the two-dimensional (2D) dynamic response of horizontally aligned, cylindrical twin tunnels subjected to vertically incident seismic waves was simulated by a finite/infinite element approach. They studied how inter-tunnel spacing affected the peak horizontal acceleration, the maximum and minimum primary stresses, and other variables. The uplift behavior and the impact of contact between twin tunnels in liquefied soil were presented by Zheng et al. (2021) using a finite difference method. The excess pore pressure and uplift displacement of twin tunnels were thoroughly analyzed, and the results were then compared to those of a single tunnel. Their study showed that the generation of excess pore pressure and the liquefaction of soil surrounding the tunnels were prerequisites for the uplift. In addition, the uplift behaviors of tunnels were affected by the interaction between twin tunnels. According to Sun et al. (2008), the tunnel's final lining system was installed during

the design earthquake. The outcomes of their simulation were consistent with those of centrifuge experiments performed by Chou et al. (2011) modeling the identical tunnel condition. The physical model testing revealed that a lot of sand was moving toward the uplifted tunnel's invert. The intensity of the input earthquake shaking and the generation of excess pore pressure were both found to have an impact on the uplift. However, the abovementioned studies simulated idealized conditions of tunnels, i.e., tunnels buried in a single liquefiable soil layer. It should be noted that tunnels are surrounded by multi-layers of both liquefiable and non-liquefiable soils. In fact, the existence of non-liquefiable soil alters how a tunnel behaves during earthquake loading.

This study focuses on how a tunnel subjected to seismic pressure and buried in both liquefiable and non-liquefiable soils responds to uplift. The finite-element method was used to perform a seismic analysis and liquefaction of the soils surrounding the tunnel. An advanced constitutive model was adopted in the finite-element model for in-depth analyses of the uplift displacement and excess pore pressure of surrounding soils.

## 2. Numerical modelling

### 2.1. General description

An idealized tunnel with an external diameter of 5 m was simulated using a finite element software Plaxis 2D. Note that the plane strain condition is commonly adopted in simulations of tunnels as it is a long straight section. A full model was 120 m wide and 40 m high, as shown in Figure 1. The model included three different soil types: sand (liquefiable soil), clay, and bed rock (the foundation). Figure 1 shows the thickness  $H = 5$  m of the non-liquefiable soil layer above the tunnel. To examine the impacts of the non-liquefiable soil thicknesses on excess pore water pressure and subsequently the tunnel uplift displacement, four case studies corresponding to four thicknesses of 15 m, 10 m, 5 m, and 0 m were used in the current work. The tunnel position was fixed and the thicknesses of the liquefiable soil layer were then 5 m, 10 m, 15 m, and 20 m for  $H = 15$  m,

$H = 10$  m,  $H = 5$  m, and  $H = 0$  m, respectively. The phreatic line was assumed to be located at the ground surface (worst-case scenario). During the construction, soil clusters inside the tunnel were set to dry condition. In addition to the dewatering of the tunnel, other construction stages, e.g., excavation of the soil, and installation of tunnel lining, were also simulated in all models. The finite element mesh of a numerical model is shown in Figure 2. A massive number of elements were generated in the areas of interest, providing the finer mesh near the tunnel. This is due to the fact that these areas would be affected by large strains during the stage of construction. The coarser mesh was then generated at the far-field areas to minimize computation time. In addition, the maximum element sizes of all models were chosen considering the maximum

frequency of the input motion spectrum and the wavelength of the propagating wave. As for the mechanical boundary conditions, the model was assumed to be fully fixed at its bottom. The horizontal displacements were assumed to be zero along the lateral edges (i.e., both left and right vertical boundaries). As for the dynamic boundary conditions, the free-field boundary was applied for the lateral edges, and a compliant base was applied for the bottom. The Kobe 1995 accelerogram was used as input ground motion (i.e., both vertical and horizontal motions in Figure 3). The input signals were scaled at peaks of horizontal and vertical accelerations of 0.55g and 0.2g, respectively. To control numerical noise, a Rayleigh damping ratio of 0.005 is used. A predetermined displacement was imposed at the bottom of the model in order to simulate the

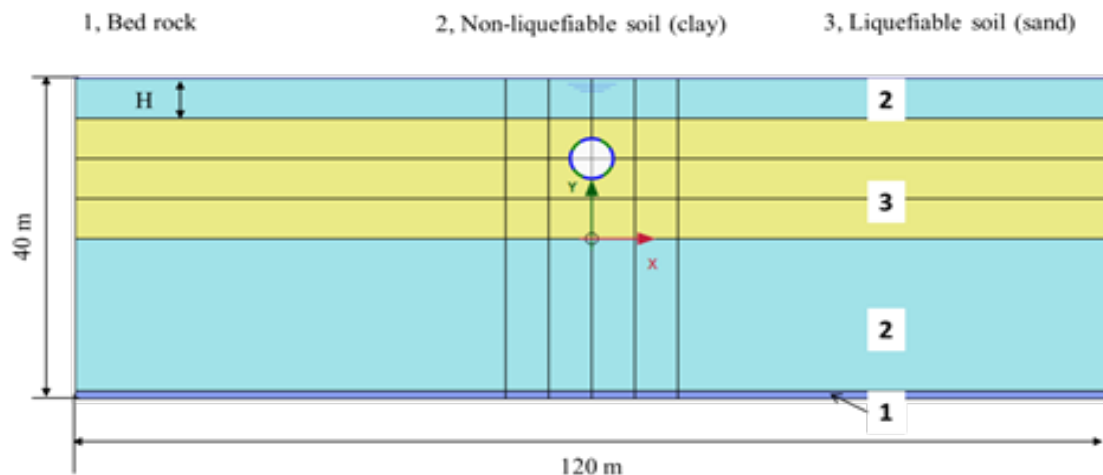


Figure 1. Selected geometry of tunnel and surrounding soil layers ( $H=5$  m).

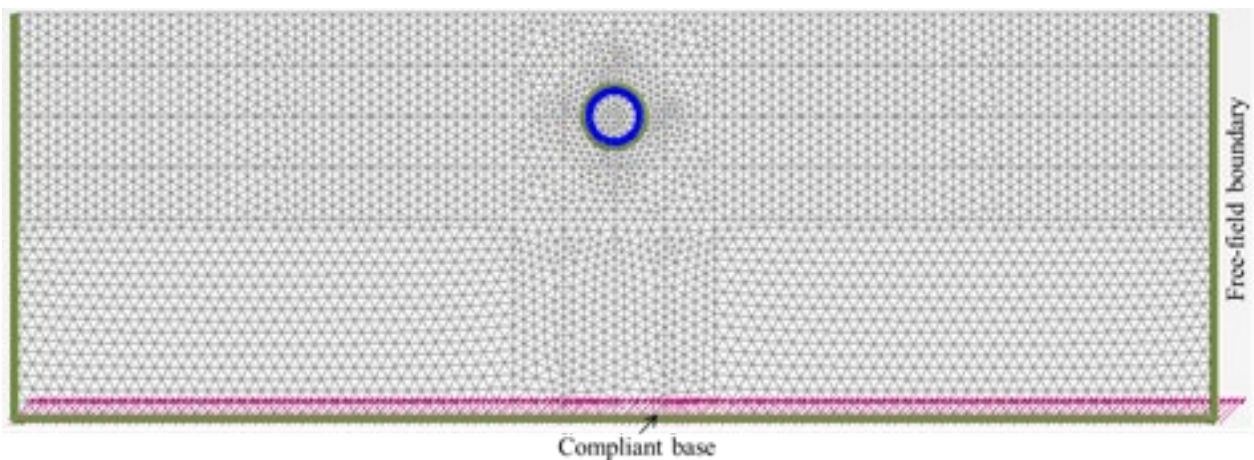


Figure 2. Finite element mesh of a numerical model.

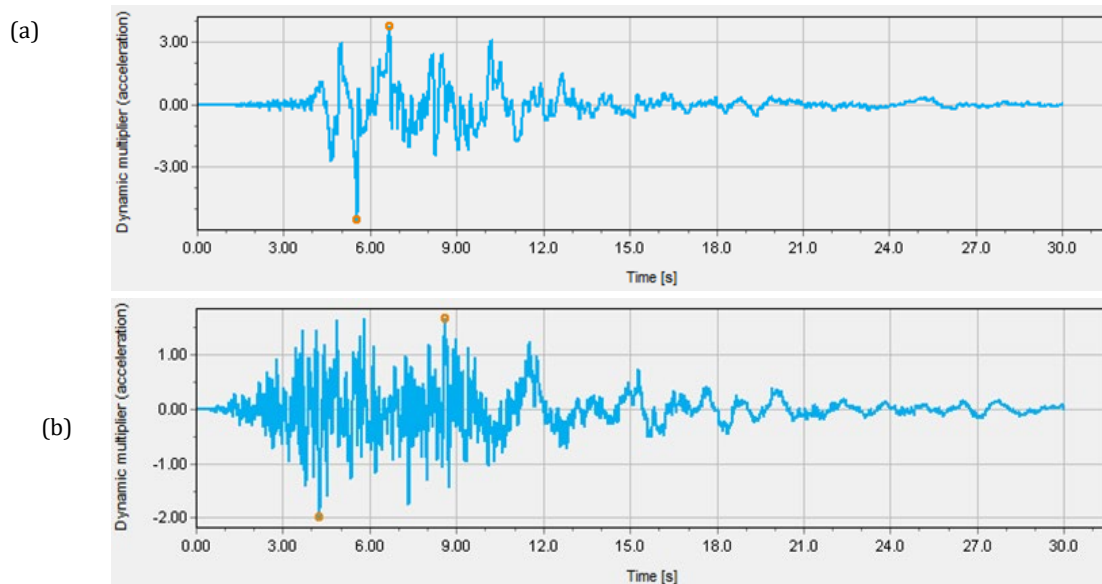


Figure 3. Time history of earthquake signals: (a) horizontal motion and (b) vertical motion.

earthquake, which was thought to be measured at the outcrop of a rock formation (Boulanger and Ziotopoulou 2015).

## 2.2. General description

In this study, the non-liquefiable soil (clay layers) was modeled using the Hardening soil small strain model (HS small), whereas the bedrock layer was modeled as the linear elastic (LE) material of drained type behavior.

## 2.3. General description

In this study, the non-liquefiable soil (clay layers) was modeled using the Hardening soil small strain model (HS small), whereas the bedrock layer was modeled as the linear elastic (LE) material of drained type behavior. The sand plasticity constitutive model (PM4Sand) was used to simulate the liquefiable soil (sand layer). The PM4Sand has successfully simulated the material behavior of liquefiable soils in dynamic or cyclic loadings, including the pore pressure generation, liquefaction, and post-liquefaction phenomena. The PM4Sand model is the elastoplastic, bounding surface plasticity, and model critical state compatible (Boulanger and Ziotopoulou 2015). It was originally proposed from the Dafalias-Manzari model (Dafalias Yannis and Manzari Majid 2004; Manzari and Dafalias, 1997) and then Boulanger and Ziotopoulou (2015) developed it extensively.

There are various inherent advantages of using the PM4Sand model for the evaluation of dynamic properties of sand (e.g., proper stress-strain and pore pressure build-up simulations, acceptable approximation of empirical correlations used in practice, including the post-liquefaction settlements, precise simulation of the accumulation of shear strain and strength modulus reduction curves, easy forecast of a number of uniform cycles to cause initial liquefaction) (Vilhar et al. 2018). In numerous earlier investigations, the PM4Sand has been utilized to examine dynamic soil-structure interactions with earthquake-induced soil liquefaction (Boulanger et al. 2018; Boulanger and Montgomery 2016; Vilhar et al. 2018; Zheng et al. 2021). In this study, input parameter values of clay and bedrock were adopted from a previous study by Vilhar et al. (2018). Input parameter values of the PM4Sand model were evaluated and calibrated based on the apparent relative density ( $D_r$ ) of sand, which is presented in detail in the report on the PM4sand model by Boulanger and Ziotopoulou (2015). All input parameter values used in the numerical analyses are tabulated in Table 1. The continuous lining was characterized by the normal stiffness  $EA = 1.4 \times 10^7$  kN/m, the flexural rigidity  $EI = 1.4 \times 10^5$  kNm<sup>2</sup>/m, weight  $w = 8.4$  kN/m/m, lining thickness  $t = 0.35$  m, and the Poisson's ratio  $\nu = 0.15$  (Brinkgreve et al. 2011).

Table 1. Parameter values of used in the numerical analyses.

Parameter	Bed rock	Clay	Sand	Unit
Constitutive model	LE	HS small	PM4 sand	-
Saturated unit weight	22	21	18	kN/m <sup>3</sup>
Unsaturated unit weight	22	19	14	kN/m <sup>3</sup>
Young's modulus	8×10 <sup>6</sup>	-	-	kN/m <sup>2</sup>
Poisson's ratio	0.2	0.2	0.3	-
Cohesion	-	26	-	kN/m <sup>2</sup>
Friction angle	-	35	33	degrees
Secant stiffness in standard drained triaxial test	-	9000	-	kN/m <sup>2</sup>
Tangent stiffness for primary oedometer loading	-	9000	-	kN/m <sup>2</sup>
Unloading - reloading stiffness	-	27000	-	kN/m <sup>2</sup>
Power for stress-level dependency of stiffness	-	1	-	-
Shear modulus at very small strains	-	60000	-	kN/m <sup>2</sup>
Shear strain at which $G_s = 0.722 G_0$	-	0.0007	-	
Failure ratio	-	0.9	-	-
Reference stress	-	100	100	kN/m <sup>2</sup>
Over-consolidation ratio	-	-	-	-
Relative density	-	-	55	%
Shear modulus coefficient	-	-	677	-
Contraction rate	-	-	0.4	-
Parameter controlling the peak stress ratio	-	-	0.5	-
Parameter controlling dilatancy	-	-	0.1	-
Maximum void ratio	-	-	0.60	-
Minimum void ratio	-	-	0.31	-

### 3. Results and discussion

#### 3.1. Soil liquefaction due to seismic loading

The excess pore pressure ratio, or  $r_u$ , which is a ratio between the excess pore water pressure and the initial vertical effective stress, can be used to represent the potential for liquefaction (Eq. 1). One of the most crucial variables for liquefaction potential analysis is the excess pore water pressure ratio ( $r_u$ ). The final pore pressure ( $u_f$ ), which is equal to the sum of the initial effective stress and the initial pore water pressure, can be determined as  $r_u$  approaches 1.0. As a result, the final effective stress  $s$ -also known as the initial liquefaction effective stress-is found to be zero.

$$r_u = \frac{\Delta p_w}{\sigma'_{v0}} = \frac{\sigma'_{v0} - \sigma'_v}{\sigma'_{v0}} = 1 - \frac{\sigma'_v}{\sigma'_{v0}} \quad (1)$$

Where  $\Delta p_w$  is excess pore water pressure;  $\sigma'_v$  is vertical effective stress and  $\sigma'_{v0}$  is initial vertical effective stress at the beginning of the dynamic calculation.

The excess pore pressure ratio at the end of the earthquake is depicted in Figure 4 (non-liquefiable soil thickness  $H = 10$  m). To assess the liquefaction potential of the soil layers surrounding the tunnel, the excess pore pressure ratio,  $r_u$ , which is reached in a soil element, is used. As can be observed, most of the liquefiable soil layer (sand) liquefied during the earthquake (i.e.,  $r_u$  reached 1.0), whereas the rest (i.e., non-

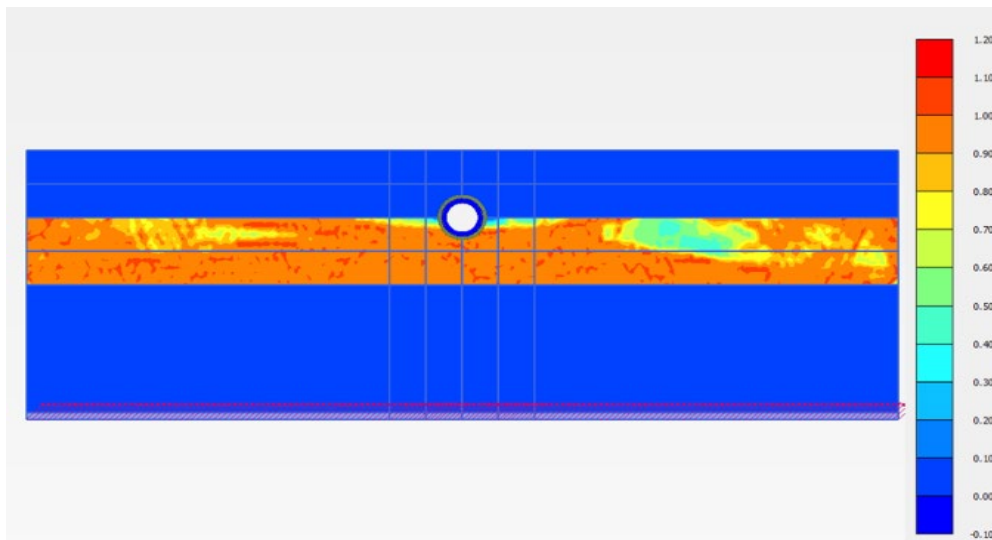


Figure 4. Excess pore pressure ratio ( $r_u$ ) of soil layers at the end of the earthquake (Case study  $H=10$  m).

liquefiable soil layers) had low  $r_u$ , i.e., no liquefaction.

Additional insight into the liquefaction potential analysis can be attained by looking into  $r_u$  of typical points B and D, as shown in Figure 5. Non-liquefiable soil is represented by point B in the middle of the clay layer, while liquefiable soil is represented by point D in the middle of the sand layer. As can be seen, the increase in  $r_u$  at point B was relatively insignificant during the earthquake (30 s). However,  $r_u$  at point D accumulated rapidly up to 1.0 (liquefaction) after about 7 s and remained high until the end of the earthquake.

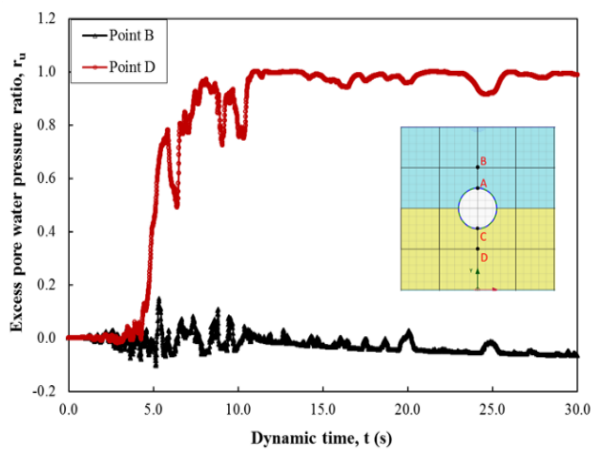


Figure 5. Excess pore pressure ratio at points B and D during the earthquake (Case study H=10 m).

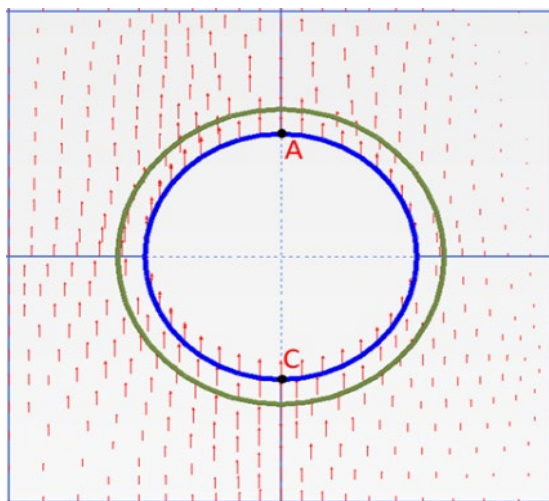


Figure 6. Spatial deformation plot produced from the numerical analysis at the end of the earthquake (Case study H=10 m).

### 3.2. Tunnel uplift displacement due to seismic loading

It is well-known that the uplift behavior of a tunnel involves the liquefaction-induced large deformation of surrounding soils. Figure 6 illustrates the spatial deformation plot produced from the numerical analysis (Case study H = 10). Relative motion and interaction zones at both ends of the tunnel can be visible as a result, which causes the tunnel to be uplifted. The liquefiable soil layer beneath the tunnel would also experience the development of excess pore water pressure during the earthquake, which would apply a force that would cause the tunnel to lift upward. A similar observation can also be found in the previous studies on tunnel uplift behavior (Chian et al. 2014; Zheng et al. 2021).

Take Point A (crown of the tunnel) and Point C (invert of the tunnel) as examples: Before 5 seconds into the earthquake, the tunnel's movement was little; after that, it began to move significantly until the end of the earthquake. Due to the seismic input motions, both settlement and uplift behaviors can be seen at this time (both vertical and horizontal motions). At the end of the earthquake, it was discovered that the tunnel's final uplift displacement was 0.078 m. Additionally, as indicated in Figure 7, it is anticipated to see the same displacement at Points A (the tunnel's crown) and C (its invert).

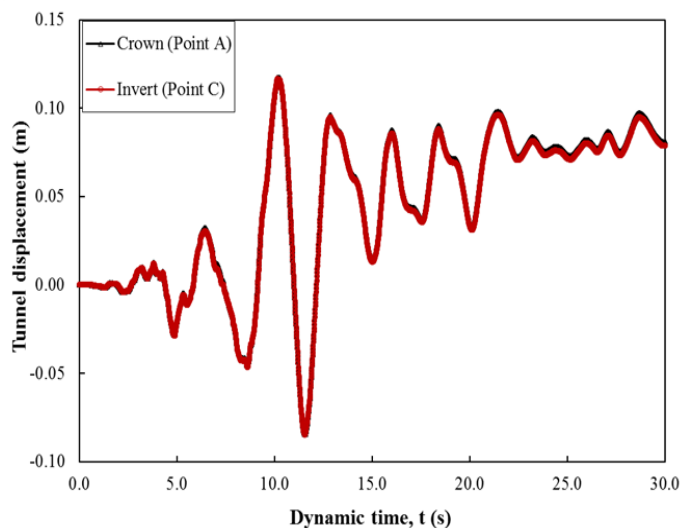


Figure 7. Tunnel uplift displacement vs time histories during the earthquake (Case study H=10 m).

### 3.3. Effects of the non-liquefiable soil thickness on the tunnel uplift displacement and excess pore water pressure

Figure 8 depicts how the thickness of the non-liquefiable soil affected the development of excess pore water pressure during the earthquake (typical point right beneath the invert of the tunnel). As demonstrated, the non-liquefiable soil thickness  $H$  had an impact on the accumulation of excess pore water pressure. Particularly, the rise in  $r_u$  during the earthquake was very negligible when the tunnel was completely buried in clay (i.e.,  $H = 15$  m) (30 s). As demonstrated in Figure 9, a negligible uplift displacement of the tunnel may result from a negligible excess pore water pressure of soil beneath the tunnel's invert. However, at the ends,

$r_u$  quickly accumulated up to around 0.5, 0.64, and 0.6 as  $H = 10$  m,  $H = 5$  m, and  $H = 0$  m, respectively. As the thickness of the non-liquefiable soil decreased, the uplift displacement increased. In this regard, the stability of the tunnel was significantly influenced by the thickness of the non-liquefiable soil  $H$ . However, because the tunnel's position and dimensions are fixed, this conclusion is encouraging for the case in this study.

### 4. Conclusions

In this study, a numerical analysis of the tunnel uplift behavior subjected to seismic loading was conducted. A tunnel buried in liquefiable and non-liquefiable soils subject to seismic loading was simulated using finite-element software. In the finite-element models,

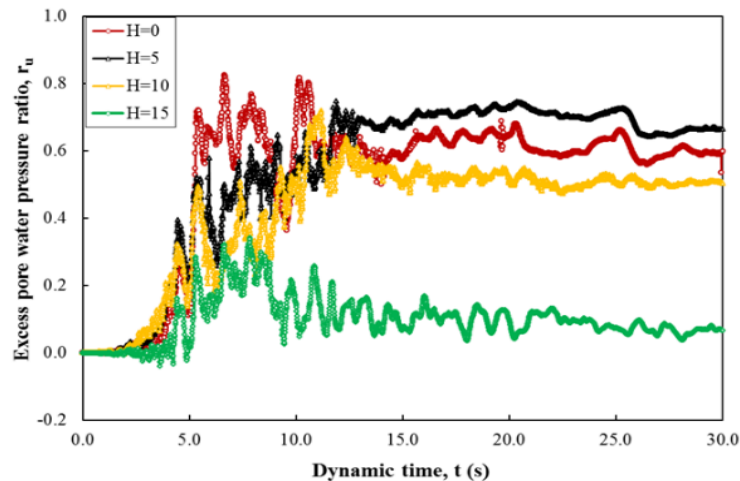


Figure 8. Effects of the non-liquefiable soil thickness on excess pore water pressure.

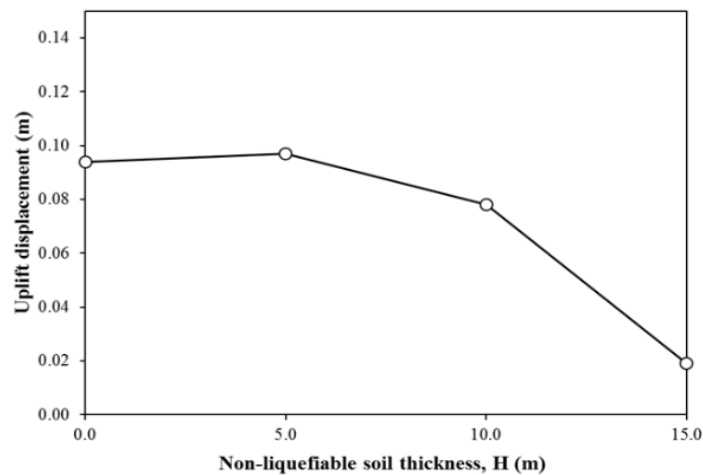


Figure 9. Effects of the non-liquefiable soil thickness on the tunnel uplift displacement.

PM4sand, an advance constitutive model for dynamic soil-structure interactions with earthquake-induced soil liquefaction, was utilized. Based on the results of this study, the following conclusions can be drawn:

- When the earthquake occurred, liquefaction mostly occurred in the liquefiable soil layer (sand;  $r_u$  reached 1.0), not in the non-liquefiable soil layers (clay layers).
- The relative motion and interaction at both ends of the tunnel caused the uplift displacement. Additionally, the tunnel's invert experienced an increase in pore water pressure.
- The tunnel uplift displacement and the development of excess pore water pressure were both considerably impacted by the thickness of the non-liquefiable soil layer- i.e., the excess pore water pressure buildup and uplift displacement increased as the thickness of the non-liquefiable soil decreased.

### Acknowledgments

This study was supported by Hanoi University of Mining and Geology, Vietnam, and Lulea University of Technology, Sweden.

### Contribution of authors

Tan Manh Do: Conceptualization, Methodology, Software, Validation, Writing-original draft preparation, Writing-review and editing; Anh Ngoc Do: Conceptualization, Methodology, Software, Validation, Writing-review and editing, Supervision; Hung Trong Vo: Conceptualization, Writing-review and editing, Supervision; All authors have read and approved the final version of the work for publication.

### References

Adalier, K., Abdoun, T., Dobry, R., Phillips, R., Yang, D., and Naesgaard, E. (2003). "Centrifuge modelling for seismic retrofit design of an immersed tube tunnel" *International Journal of Physical Modelling in Geotechnics*, 3(2), 23-35.

Azadi, M., and Hosseini, S. M. M. (2010). "The uplifting behavior of shallow tunnels within the liquefiable soils under cyclic loadings." *Tunnelling and Underground Space Technology*, 25(2), 158-167.

Boulanger, R., and Ziotopoulou, K. (2015). *PM4Sand (Version 3): A sand plasticity model for earthquake engineering applications*. Center for Geotechnical Modeling Report No. UCD/CGM-15/01, Department of Civil and Environmental Engineering, University of California, Davis, Calif.

Boulanger, R. W., Khosravi, M., Khosravi, A., and Wilson, D. W. (2018). Remediation of liquefaction effects for an embankment using soil-cement walls: Centrifuge and numerical modeling. *Soil Dynamics and Earthquake Engineering*, 114, 38-50.

Boulanger, R. W., and Montgomery, J. (2016). Nonlinear deformation analyses of an embankment dam on a spatially variable liquefiable deposit. *Soil Dynamics and Earthquake Engineering*, 91, 222-233.

Brinkgreve, R., Swolfs, W., Engin, E., Waterman, D., Chesaru, A., Bonnier, P., and Galavi, V. (2018). "PLAXIS 2D Reference manual." *Delft University of Technology and PLAXIS bv The Netherlands*.

Chian, S. C., Tokimatsu, K., and Madabhushi, S. P. G. (2014). Soil liquefaction-induced uplift of underground structures: Physical and numerical modeling. *Journal of Geotechnical and Geoenvironmental Engineering*, 140(10), 04014057.

Chou, J., Kutter, B., Travasarou, T., and Chacko, J. (2011). Centrifuge modeling of seismically induced uplift for the BART transbay tube. *Journal of Geotechnical and Geoenvironmental Engineering*, 137(8), 754-765.

Dafalias Yannis, F., and Manzari Majid, T. (2004). Simple Plasticity Sand Model Accounting for Fabric Change Effects. *Journal of Engineering Mechanics*, 130(6), 622-634.

Manzari, M. T., & Dafalias, Y. F. (1997). A critical state two-surface plasticity model for sands. *Géotechnique*, 47(2), 255-272.

Hu, J., Chen, Q., and Liu, H. (2018). Relationship between earthquake-induced uplift of rectangular underground structures and the excess pore water pressure ratio in saturated sandy soils. *Tunnelling and Underground Space Technology*, 79, 35-51.

- Lin, S.-Y., Hung, H.-H., Yang, J. P., and Yang, Y. (2017). Seismic analysis of twin tunnels by a finite/infinite element approach. *International Journal of Geomechanics*, 17(9), 04017060.
- Liu, H., and Song, E. (2006). Working mechanism of cutoff walls in reducing uplift of large underground structures induced by soil liquefaction. *Computers and Geotechnics*, 33(4-5), 209-221.
- Saeedzadeh, R., and Hataf, N. (2011). Uplift response of buried pipelines in saturated sand deposit under earthquake loading. *Soil Dynamics and Earthquake Engineering*, 31(10), 1378-1384.
- Sun, Y., Klein, S., Caulfield, J., Romero, V., and Wong, J. (2008). Seismic analyses of the Bay Tunnel. *Geotechnical Earthquake Engineering and Soil Dynamics IV*, 1-11.
- Tobita, T., Kang, G.-C., and Iai, S. (2011). Centrifuge modeling on manhole uplift in a liquefied trench. *Soils and foundations*, 51(6), 1091-1102.
- Unutmaz, B. (2016). Liquefaction potential of soils around circular double tunnels. *Bulletin of Earthquake Engineering*, 14(2), 391-411.
- Vilhar, G., Laera, A., Foria, F., Gupta, A., and Brinkgreve, R. B. (2018). Implementation, Validation, and Application of PM4Sand Model in PLAXIS. *Geotechnical Earthquake Engineering and Soil Dynamics V: Numerical Modeling and Soil Structure Interaction*, American Society of Civil Engineers Reston, VA, 200-211.
- Vilhar, G., Laera, A., Foria, F., Gupta, A., and Brinkgreve Ronald, B. J. (2018). Implementation, Validation, and Application of PM4Sand Model in PLAXIS. *Geotechnical earthquake engineering and soil dynamics V, June*, 10-13
- Zheng, G., Yang, P., Zhou, H., Zhang, W., Zhang, T., and Ma, S. (2021). Numerical Modeling of the Seismically Induced Uplift Behavior of Twin Tunnels. *International Journal of Geomechanics*, 21(1), 04020240.